C Garcia-Rosales et al.

Self-passivating tungsten alloys of the system W-Cr-Y: characterization and testing

Preprint of Paper to be submitted for publication in Proceedings of 29th Symposium on Fusion Technology (SOFT 2016)

Self-passivating W-Cr-Y alloys: characterization and testing

Aida Calvo*[a], Carmen García-Rosales[a], Nerea Ordás[a], Iñigo Iturriza[a], Karsten Schlueter[b], Freimut Koch[b], Gerald Pintsuk[c], Elena Tejado[d], José Ygnacio Pastor[d],

[a]Ceit-IK4 and TECNUN (University of Navarra), E-20018 San Sebastián, Spain
[b]Max-Planck-Institut für Plasmaphysik, D-85748 Garching, Germany
[c]Forschungszentrum Jülich GmbH, D-52425 Jülich, Germany
[d]Polytechnic University of Madrid, E-28040 Madrid, Spain

The use of self-passivating tungsten alloys for the first wall armor of future fusion reactors is advantageous concerning safety issues in comparison with pure tungsten. Bulk W-10Cr-0.5Y alloy manufactured by mechanical alloying followed by HIP resulted in a fully dense material with grain size around 100 nm and a dispersion of Y-rich oxide nanoparticles located at the grain boundaries. An improvement in flexural strength and fracture toughness was observed with respect to previous works. Oxidation tests under isothermal and accident-like conditions revealed a very promising oxidation behavior for the W-10Cr-0.5Y alloy. Thermo-shock tests at JUDITH-1 to simulate ELM-like loads resulted in a crack network at the surface with roughness values lower than those of a pure W reference material. An additional thermal treatment at 1550 °C improves slightly the oxidation and thermo-shock resistance of the alloy.

Keywords: tungsten, self-passivating alloy, oxidation behavior, yttrium, thermo-shock

1. Introduction

In future fusion reactors such as DEMO, a potential loss-of-coolant (LOCA) accident with simultaneous air ingress into the vacuum vessel would involve temperatures of the components above 1000 °C because of the decay heat. [1]. Pure tungsten is the main candidate for the first wall armor [2]. However, under accident conditions the use of pure tungsten would lead to the formation of activated and volatile tungsten oxides, representing an important safety risk [3]. It has been demonstrated that the addition of oxide forming alloying elements to pure tungsten results in the growth of a stable protective oxide scale that prevents tungsten from oxidation at high temperatures in presence of oxygen [4–6]. Under normal operation the surface of these self-passivating alloys will consist of pure tungsten due to preferential sputtering of the alloying elements.

A recent work [7] based on previous results [6, 8] demonstrates that a tungsten alloy of composition W-12Cr-0.5Y leads to a significant reduction of oxidation rate at temperatures ≤ 1000 °C, compared to those of the binary W-Cr and previously studied ternary systems. Furthermore, the dispersion of Y-rich nanoparticles observed at grain boundaries (GB) of the W matrix, refines the grain size distribution and is expected to improve the mechanical properties as reported in different works [9, 10]. Previous works also show that a reduction of the Cr concentration in binary W–Cr alloys from 15 to 10 wt% Cr reduces the oxidation rate [8].

In this work, a new alloy of composition W-10Cr-0.5Y is manufactured by mechanical alloying (MA) and densified by Hot Isostatic Pressing (HIP). The alloy is subjected to a subsequent thermal treatment (TT) to dissolve the Cr-rich phase and achieve a single bcc phase [7], in agreement with the W-Cr phase diagram [11]. Microstructural investigations and microhardness of the alloy after HIP and after the TT are presented and compared to the W-12Cr-0.5Y alloy. Thermal conductivity and flexural strength of as-HIPped material are also shown. Results of oxidation tests at various conditions and thermo-shock tests at JUDITH-1 (Juelich Divertor Test Facility Hot Cells) [12] are included.

2. Experimental details

Elemental powders of pure W (99.95%, 15-30 μm), Cr (99.95%, 74 μm) and Y (99.9%, 20-30 μm) were used to produce samples of composition W-10Cr-0.5Y in wt.%. The starting powders were mechanically alloyed under Ar in a planetary ball mill using WC grinding jars and balls. The MA parameters were those found as optimum for the W-Cr-Y system in [7]. Metallic capsules with the alloyed powder were evacuated, degassed, sealed and HIPed at 1250 ºC for 2 h at 150 MPa. A thermal treatment on HIPed samples was performed at 1550 ºC under H_2. The oxygen and nitrogen contents of powders and bulk materials were determined using the inert gas fusion method (ASTM E1569), and the carbon content by the combustion method (ASTM E1019). Powders and bulk samples were characterized by field emission gun (FEG)-SEM and energy dispersive X-ray spectroscopy (EDS). The relative density of the samples was determined from the geometrical and theoretical densities. The average grain size of dense materials was determined by quantitative metallography. Vickers microhardness was measured applying a load of 0.5 kg for 5 seconds. Three-point bending tests (3PBT) were performed on smooth and single edge laser-notched beams [13] (nominal dimensions $1.8 \times 1.8 \times 20$ mm³) over the temperature range 20 °C to 1100 °C under high vacuum. All tests were performed in displacement control at a fixed loading rate of 100 μm/min with 16 mm span width. Flexural strength was computed by Euler–Bernoulli equations for slender beams up to failure. To calculate the fracture toughness (K_{IC}), the maximum load and the initial notch length for each test, measured previously via FEG-SEM, were computed in the formula proposed by Guinea et al [14]. The thermal conductivity was obtained by the laser flash

method. Isothermal oxidation tests at 800 °C and 1000 °C for up to 60 h were performed by thermogravimetric analysis (TGA). Tests under accident-like conditions, described in [7], were also done. Surfaces and cross sections of the oxidized samples were analyzed by FEG-SEM and Focused Ion Beam (FIB). Thermo-shock tests were performed at the electron beam facility JUDITH-1 [12] on samples of dimensions $10 \times 10 \times 4$ mm^3, which were exposed at a base temperature of 400 °C to ELM-like loads consisting of 1000 pulses with power densities of 0.19 and 0.38 GW/m^2 for 1 ms, and to a disruption-like load of 1.13 GW/m^2 for 5 ms. To ensure a homogeneous loading, a small area (4×4 mm^2) was scanned with a focused electron beam at very high scanning frequencies. After exposure, the surface and cross section of the samples were investigated by optical microscopy.

3. Results and discussion

The relative density and the O, C and N contents of the W-10Cr-0.5Y alloy after HIP and after TT (Table 1) are comparable to those obtained in previous works for the W-12Cr-0.5Y alloy [7].

3.1. Microstructure

After HIP, a very fine and homogeneous microstructure can be appreciated (Fig. 1 (a)), with two main phases identified by EDS as a W-rich phase with Cr in solution ((αW,Cr), bright grey majority phase) and a Cr-rich phase with W in solution ((αCr,W), dark grey discontinuous phase). This microstructure is consistent with the predictions of the W-Cr phase diagram at 1250 °C [11]. The average grain size of the matrix is about 100 nm, considerably finer than that of the W-15Cr binary system, since Y acts as grain growth inhibitor, as reported in [7, 15]. A dispersion of Y-rich oxide nanoparticles of about 15 nm size is formed mainly at the GB as a result of the decomposition of less stable oxides during HIPing and the high oxygen affinity of Y. This cleaning effect of GB from oxygen together with the grain refinement are supposed to be beneficial for improving the strength and toughness of the alloy at high temperature [9, 15–17].
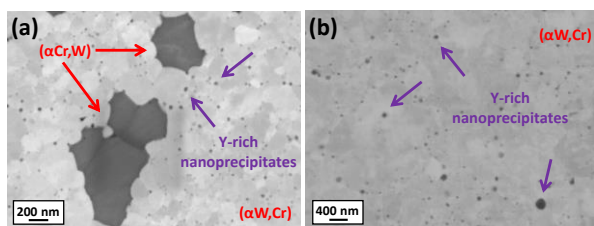

Fig. 1. FEG-SEM images of W-10Cr-0.5Y alloy (a) after HIP and (b) after HIP + TT at 1550 °C

The microstructure after TT at 1550 °C is shown in Fig. 1 (b) and consists of a single (αW,Cr) phase, as expected from the W-Cr phase diagram. Residual particles of (αCr,W) phase can be also found. As a consequence of the TT grain growth up to approximately 230 nm is observed in the matrix, as well as a thickening of the Y-rich oxide nanoparticles, up to about 50 nm. Further work is required to identify by TEM the composition of these nanoparticles.

3.2. Microhardness and thermal conductivity

The Vickers microhardness of W-10Cr-0.5Y alloy after HIP and after TT at 1550 °C is listed in Table 1. As reference, the microhardness of pure polycrystalline W at the corresponding average grain size is included, taking into account its Hall-Petch relationship [18]. The hardness of the as-HIPed alloy and the alloy after TT are slightly lower than that of pure W at the same average grain size, as might be expected because of the presence of a Cr-rich phase with lower hardness than W after HIP. These values are also comparable with previous results [7, 19] and show the influence of grain size on hardening.

The thermal conductivity of W-10Cr-0.5Y alloy at the operation temperature (~600 °C) is about 56 W/mK. It is lower than that of pure W due to the fact of alloying. Nevertheless, alloys of the W-Cr-Y system exhibit the highest thermal conductivity of all ternary alloys evaluated previously [7, 19].

3.3. Mechanical properties

Non-standard 3PBT were performed on as-HIPed W-10Cr-0.5Y alloy from 25 °C to 1100 °C to explore its mechanical response. As can be observed in Fig. 2 the specimens showed brittle behavior up to 900 °C while some plastic deformation took place at 950 ºC, therefore the ductile-to-brittle transition temperature (DBTT) lies between 900 ºC and 950 ºC. Although the W-Cr-Ti system presented a similar DBTT [19, 20], a decrease was expected taking into account the grain size reduction [21], but there is no variation though. On the other hand, a considerable increase in flexural strength and fracture toughness at high temperature (Table 2) was observed with respect to previous works [19, 20], probably because of grain refinement and improvement in the MA process. The results of 3PBT showed that the behavior of the alloy was linear elastic until fracture up to 1050 ºC, temperature from which the samples exhibited plastic deformation without breaking. The primary effect of nano-dispersed Y-rich oxides in W is an increase in strength, elastic modulus and fracture toughness by inhibiting the degradation at higher temperatures as reported in [17, 22].
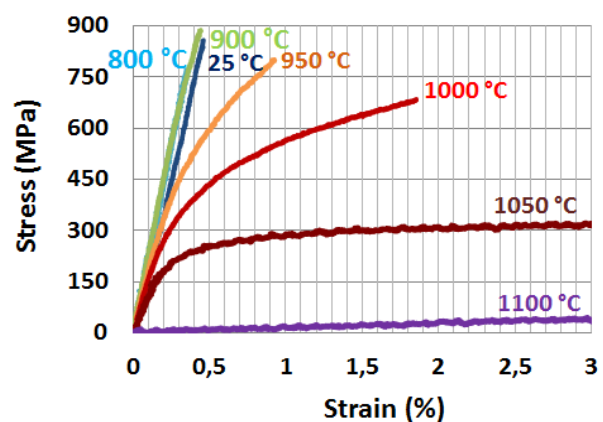

Fig. 2. Flexural strength vs strain of W-10Cr-0.5Y alloy as HIPed from 25 °C up to 1100 °C

Table 1. Relative density, impurities content, average grain size, microhardness and thermal conductivity of the W-Cr-Y alloys after HIP and after TT. For comparison, the microhardness of pure polycrystalline tungsten at the same average grain size is included.

Alloy	Relative Density (%)	Impurities (ppm)			Average grain size (nm)	Microhardness		Thermal conductivity at 600 ° C (W/mK)
		O	N	C		Alloys (HV$_{0.5}$)	Pure W (HV) [18]	
W-12Cr-0.5Y [7]	99	1300 ± 200	90 ± 10	170 ± 10	87 ± 2	1228 ± 5	1422	55
W-10Cr-0.5Y	100	1150 ± 32	110 ± 9	140 ± 9	110 ± 4	1220 ± 8	1304	56
W-10Cr-0.5Y After TT	99	1130 ± 78	110 ± 12	160 ± 15	230 ± 11	980 ± 6	1009	-

Table 2. Fracture toughness of W-10Cr-0.5Y alloy as HIPed

T(ºC)	25	800	900	1000	1100
F. Tough. (MPa·m$^{0.5}$)	5.2	6.0	6.1	7.2	8.5
Std. Error (MPa·m$^{0.5}$)	0.1	0.6	0.9	2.0	0.3

3.4. Oxidation tests

Isothermal oxidation tests at 800 ºC and 1000 ºC for 60 h as well as tests under accident-like conditions up to 1000 ºC were performed with the as-HIPed and HIP+TTed W-0Cr-0.5Y alloy. The mass gain during isothermal oxidation at both temperatures follows a linear kinetics with an initial parabolic phase. The oxidation rates obtained for this alloy are the lowest of all bulk systems studied so far, even lower than those for W-12Cr-0.5Y [6, 7] as can be observed in Table 3.

The surface of the W-10Cr-0.5Y isothermally oxidized at 1000 ºC and the cross section of the formed scales were analyzed by FEG-SEM, FIB and EDS (Fig. 3). At the surface, particles of Cr_2WO_6 of ~1 μm and W-Y mixed oxides of about 2 μm can be observed partly covering the thin Cr_2O_3 layer consisting of nanoparticles (light grey, white and black particles respectively, in Fig. 3 (a)). In the cross sections of the oxidized surfaces (Fig. 3 (b)) three layers can be distinguished: a thin Cr_2O_3 scale partly covered with W-Y mixed oxide particles at the very surface and a thin Cr_2WO_6 layer just below, followed by a thicker WO_3 layer. It seems that the W-Y-O particles reinforce the protecting effect of the Cr_2O_3 scale leading to oxidation layers of about 14 μm thick, which is consistent with the low mass gain observed. Partial oxidation of the Cr-rich phase located near the scales was also observed. After 60 h oxidation at 800 ºC the particles on the oxidized surface are smaller and the scales are thinner with an overall thickness of ~500 nm.

In contrast to the isothermal oxidation, mass increase of W-10Cr-0.5Y alloy at the second isothermal segments during the accident-like test follows a parabolic law and this alloy exhibits the best behavior against oxidation of all tested systems including W-12Cr-0.5Y alloy [6, 7] as can be observed in Fig. 4. Samples subjected to TT were also studied showing a slight decrease in mass gain with respect to the as-HIPed material. Another important observation is the fact that in the isothermal segments without oxygen there is no mass loss, indicating that there is no evaporation of tungsten oxide, previously formed during the oxidation segment. The surface and oxidation scales after accident-like condition test are similar to those of Fig. 3 but the thickness and particle sizes are smaller since the overall exposition time at 1000 ºC under oxidizing atmosphere is 2 hours instead of 60 hours in isothermal tests.

Table 3. Linear oxidation rates, k$_L$, of W-10Cr-0.5Y alloy and comparison with alloys of previous results [6, 7].

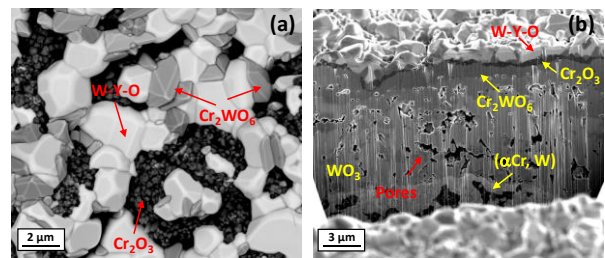| Alloy	k$_L$ [mg/(cm2·s)]	
	800 ºC	1000 ºC
W-15Cr	2.9 · 10^{-4}	Delamination
W-10Cr-2Ti	4.7 · 10^{-6}	Delamination
W-12Cr-0.5Y	3.1 · 10^{-6}	-
W-10Cr-0.5Y	3.9 · 10^{-7}	7.5 · 10^{-6}

Fig. 3. FIB images of (a) surface and (b) cross section of W-10Cr-0.5Y alloy after oxidation tests at 1000 °C for 60h
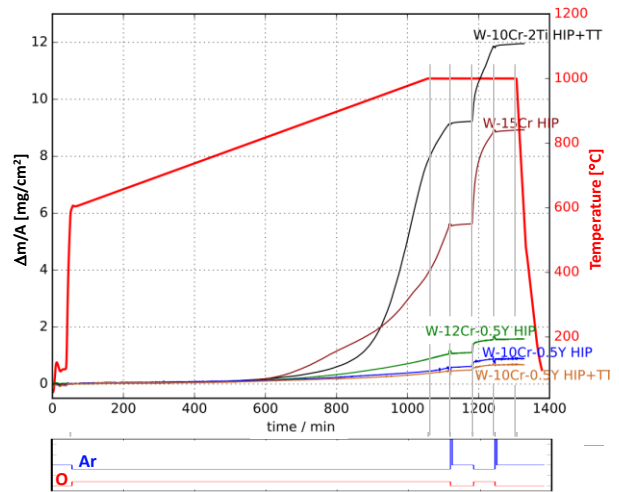

Fig. 4. Mass increase per unit area during accident-like conditions test of W-10Cr-0.5Y alloy as-HIPed and after TT compared to previous works [6, 7]

3.5. Thermo-shock tests

W-10Cr-0.5Y alloy as-HIPed and after TT was exposed to ELM-like loads. After 1000 heat pulses of 0.19 GW/m^2 for 1 ms at 400 ºC no damage was detected at the surface of the samples. After 1000 pulses of 0.38 GW/m^2 a crack network appeared in both samples with no chipping as can be observed in Fig. 5. Surface roughness was reduced respect to a pure W grade reference material (IGP W) [23] under the same conditions from 0.52 μm to 0.32 μm and 0.26 μm in as-HIPed and HIP+TTed materials

respectively. The depth of cracks has not been measured yet but apparently cracks in the material after TT are narrower compared to as-HIPed material, even after disruption-like load. In this later case, partial melting was observed but no catastrophic failure in contrast to the results obtained in preliminary works [19].
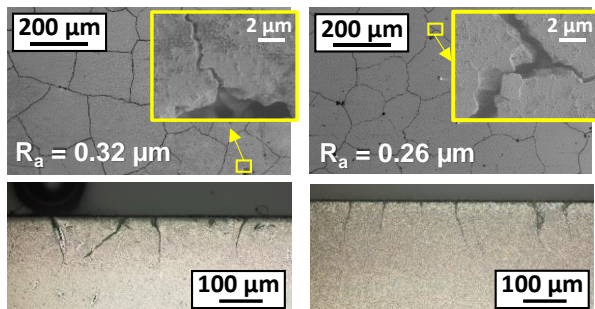

Fig. 5. Surface and cross section of W-10Cr0.5Y alloy after loading at JUDITH-1 with 1000 ELM-like pulses of 0.38 GW/m^2 for 1ms (left) as-HIPed and (right) after TT at 1550 ºC

The alloy presents an improved performance to thermal shock loading which is likely due to the reinforcement attained in both strength and toughness at high temperatures. The very fine microstructure and the presence of Y-rich oxide nanoparticles together with the slightly higher thermal conductivity might be responsible for this improvement. The TT may also contribute to improve the thermo-shock resistance since only a single phase is present in the material which leads to stress relief.

4. Conclusions

A fully dense self-passivating alloy of composition W-10Cr-0.5Y (in wt.%) was produced by MA and HIP showing a very homogeneous and nanocrystalline microstructure with average grain size ~100 nm. A Y-rich oxide nanoparticles dispersion located mainly at GB inhibits grain growth and contributes to increase the strength and toughness at high temperature, which improves the material behavior under thermo-shocks loading compared to pure W reference material. The alloy exhibits the lowest oxidation rates of all developed systems, probably owing to the W-Y oxide particles formed at the surface which improve the self-passivating effect of the Cr_2O_3 scale. A final TT at 1550 ºC seems to improve the behavior of the alloy under oxidation and thermal shock conditions. In view of all results, W-Cr-Y system is a promising first-wall armor material.

Acknowledgments

References

[1] D. Maisonnier et al., A Conceptual Study of Commercial Fusion Power Plants, Final Report. 2005.

[2] R. Neu et. al., Advanced tungsten materials for plasma-facing components of DEMO and fusion power plants, Fusion Engineering and Design 109-11 A (2016) 1–7.

[3] N. Taylor et al., Activation properties of tungsten as a first wall protection in fusion power plants, Fusion Engineering and Design 81 (2006) 1333–1338.

[4] P. López et al., Manufacturing of self-passivating W-Cr-Si alloys by mechanical alloying and HIP, Fusion Engineering and Design 86 (2011) 1719–1723.

[5] F. Koch et al., Oxidation behavior of silicon-free tungsten alloys for use as the first wall material, Physica Scripta T145 (2011) 14019.

[6] C. García-Rosales et al., Oxidation behaviour of bulk W-Cr-Ti alloys prepared by MA and HIPing. Fusion Engineering and Design 89 (2014) 1611–1616.

[7] A. Calvo et al., Manufacturing and testing of self-passivating tungsten alloys of different composition, Nuclear Materials and Energy 0 (2016) 1–8.

[8] J. Brinkmann, Personal communication., Garching 2015.

[9] M. Zhao et al., Effect of rare earth elements on the consolidation behavior and microstructure of tungsten alloys, International Journal of Refractory Metals and Hard Materials 48 (2015) 19–23.

[10] M. Battabyal et. al, Investigation of microstructure and mechanical properties of W-Y and W-Y2O3 materials fabricated by powder metallurgy method. International Journal of Refractory Metals and Hard Materials 50 (2015) 210–216.

[11] W-Cr phase diagram. Bull Alloy Phase Diagrams, (1984)

[12] R. Duwe and W. Kühnlein, The new electron beam facility for materials testing in hot cells-design and preliminary experience, Fusion Technology 1994, (1995) 355–358.

[13] T. Palacios and J. Pastor, International Journal of Refractory Metals and Hard Materials, Influence of the notch root radius on the fracture toughness of brittle metals: Nanostructure tungsten alloy, a case study, International Journal of Refractory Metals and Hard Materials 52 (2015) 44–49.

[14] G. Guinea et al., Stress intensity factor, compliance and CMOD for a general three-point-bend beam, International Journal of Fracture 5 (1998) 103–116.

[15] M. Zhao et al. The investigation of Y doping content effect on the microstructure and microhardness of tungsten materials, Mater Science and Engineering A 618 (2014) 572–577.

[16] B. Gludovatz et al., Influence of impurities on the fracture behaviour of tungsten, Philosophical Magazine 91 (2011) 3006–3020.

[17] T. Palacios et al., Mechanical characterisation of tungsten – 1 wt .% yttrium oxide as a function of temperature and atmosphere, Journal of Nuclear Materials 454 (2014) 455–461.

[18] E. Lassner and W. Schubert, Tungsten: Properties, chemistry, technology of the element, alloys and chemical compounds, Austria, 1999.

[19] A. Calvo A et al., Manufacturing of self-passivating tungsten based alloys by different powder metallurgical routes, Physica Scripta T167 (2016) 14041.

[20] P. López-Ruiz et al., Powder metallurgical processing of self-passivating W alloys for fusion first wall application, Journal of Nuclear Materials 442 (2013) 219-224.

[21] J. Reiser et al., Ductilisation of W: On the shift of the brittle-to-ductile transition (BDT) to lower temperatures through cold rolling, International Journal of Refractory Metals and Hard Materials 54 (2016) 351–369.

[22] D. Blagoeva et al., Development of W and W alloys for DEMO divertor applications via MIM technology, Journal of Nuclear Materials 442 (2013) 198–203.

[23] M. Wirtz et al., Thermal shock tests to qualify different tungsten grades as plasma facing material, Physica Scripta T167 (2016) 14015.